ACS APPLIED MATERIALS & INTERFACES

Letter

www.acsami.org

High Raman Enhancing Shape-Tunable Ag Nanoplates in Alumina: A Reliable and Efficient SERS Technique

Debrina Jana, Abhijit Mandal, and Goutam De*

Nano-Structured Materials Division, CSIR-Central Glass & Ceramic Research Institute, 196, Raja S. C. Mullick Road, Kolkata 700032, India

Supporting Information

ABSTRACT: Shape-tunable Ag nanoplates in alumina enable very strong SERS performances showing Raman enhancement factor >1 × 10^9, and allows for easy detection of analyte methylene blue having a concentration in the picomolar range. Raman enhancements have been systematically studied during the Ag nanoparticle-shape evolution from spherical nanoparticles to hexagonal nanoplates with sharp corners to truncated triangular nanoplates in alumina sol. Large SERS enhancement has been observed because of the uniform dispersion and embedment of Ag nanoplates in a relatively high dielectric alumina network where analyte molecules are held. This new approach gives uniform and strong SERS signal with reproducibility.

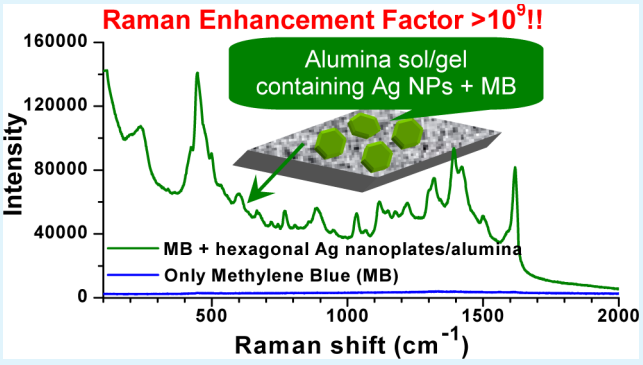

KEYWORDS: *Ag nanoplates, SERS, low concentration detection, methylene blue, enhancement factor*

Surface-enhanced Raman scattering (SERS) is a well-established phenomenon that can enhance Raman signals of nonresonant molecules adsorbed on noble metal particles by several orders of magnitude. In recent years an enormous amount of effort has been expanded in developing new and reliable techniques for SERS.[1−6] Many kinds of active substrates were developed for SERS studies, e.g., colloids,[7] electrochemically roughened electrodes,[8] vapour-deposited metal island films,[9] and lithography produced nanostructures.[10] Colloidal Au and Ag nanoparticles (NPs) have been extensively studied as SERS materials because of their unique surface plasmon resonance (SPR) features, which have exhibited application potential as active substrates for SERS.[11] However, the utility of this class of SERS materials can be limited by poor control over particle aggregation, leading to low reproducibility and variations in SERS intensities over time.

The controllable preparation of metal NPs with different shapes is also of great interest because it allows one to fine tune the SPR properties which in turn affect the SERS. While the uses of colloidal SERS substrates are widespread, studies of substrates with different shape-morphologies are limited despite their shape-dependent optical properties, which make them attractive candidates. Moreover, fabrication of reliable SERS substrate with uniformly high enhancement factors still remains a challenge.

In this letter, we demonstrate a simple and easy protocol to prepare a SERS active substrate which can detect very trace amount of analyte molecules with reproducibility. Here a different approach regarding the preparation of Ag NPs was followed which consists of the generation of Ag NPs in an alumina sol and gradual shape transformation from initially formed spherical to hexagonal and finally filleted triangular plate-like NPs. These different-shaped Ag NPs containing alumina sols were directly used for SERS experiments. It is noteworthy that SERS investigation of Ag NPs containing any dielectric matrix sol especially alumina has not been attempted so far though SERS active substrate based on porous alumina membranes has been reported.[12−14]

The approach described in this letter is completely new and advantage of this process is that the analyte can be mixed thoroughly with the active NPs in liquid state. The dropcast liquid mixture will form a gel like solid after evaporation of solvent and can be analyzed easily for Raman. Because of the homogeneous mixing in liquid state, our SERS substrate shows homogeneous SERS signal which is advantageous over bare NPs. Moreover, embedment of Ag NPs in a relatively high dielectric alumina is expected to cause enhancement of SPR intensity and thereby the SERS signal.[15,16] In this study, we use methylene blue (MB) as the probe molecule to investigate the SERS properties of the Ag NPs containing alumina sols at their different shapes and also in the intermediate stages formed during shape conversion to explore the influence of their shape on SERS enhancement. This method exhibits large Raman enhancement ability and good SERS reproducibility, enabling low concentration detection of analyte MB.

Received: May 4, 2012
Accepted: June 25, 2012
Published: June 25, 2012

Stable and dispersed Ag NPs containing alumina sols were prepared using our reported method.[17,18] In brief, first, a partially acetylacetonato (0.5 mol) complexed aluminium tri-sec butoxide (1 mol) stock solution was prepared which was named as $ASB_{0.5acac}$. After the addition of $AgNO_3$ (0.2 mol % with respect to the equivalent amount of $AlO_{1.5}$) to the $ASB_{0.5acac}$ solution, the faintly straw color sol gradually became intense yellow showing a SPR absorption at 429 nm as spherical Ag NPs were generated spontaneously through the reduction of Ag^+ to Ag^0 by Al-alkoxide (designated as yellow sol). Addition of Polyvinylpyrrolidone (PVP, average molecular weight 10 000 g/mol) 5×10^{-3} mol % with respect to the equivalent amount of $AlO_{1.5}$ at this stage caused generation of a second absorption band near 640 nm while retaining the original SPR band at 427 nm. With time, the 640 nm band gradually red shifted to 795 nm resulting a intense green sol (designated as green sol). After some time the 795 nm band was again blue shifted and stabilized at 660 nm, and a blue-colored sol (designated as blue sol) was resulted. The UV-visible spectral changes during such shape conversion along with representative photos of sols are shown in Figure S1 (see the Supporting Information). Such systematic color changes were due to the conversion of spherical NPs (yellow sol) to mainly hexagonal (with occasional triangular) nanoplates (green sol), and finally to truncated/filleted triangular Ag nanoplates (blue sol). It is noteworthy here that the atomic concentration of Ag remains same and the sol remains transparent and homogeneous during such shape evolution. Interaction strength between PVP and different crystallographic facets of silver are substantially different, which leads to such anisotropic growth of silver from spherical NPs. It is known that PVP binds preferentially on the {100} crystalline face of Ag rather than the {111} face. This directs the controlled growth of specific facets compared to other facets resulting in different plate shaped NPs and their further growth.[17,19] TEM shows existence of spherical Ag NPs of average size 12 nm in yellow sol (Figure 1a). The green sol shows presence of mainly hexagonal nanoplates having sharp corners and edges in the size ranges 145−180 nm (Figure 1b), whereas in the blue sol, relatively smaller truncated/filleted triangular nanoplates in the size range of 80−120 nm (Figure 1c) are found to exist.[17,18] In both the cases presence of a small fraction of smaller NPs are also observed; the overall size distributions of NPs are shown in Figure S2 (see the Supporting Information). AFM (see Figure S3 in the Supporting Information) and TEM (see Figure S4 in the Supporting Information) reveal that the thickness (t) of haxagonal nanoplates is lower ($t \approx 12.5$ nm) than the truncated/filleted triangular nanoplates ($t \approx 18$ nm), whereas the nanoscale rms surface roughness of these nanoplates are found to be 1.77 and 1.64 nm (see AFM line scans in Figure S3 in the Supporting Information), respectively.

MB was chosen as analyte to study the Raman activities because of its low fluorescence quantum yield (0.02 ± 0.005)[20] and it is known to form well-defined monolayer on the silver surface with a characteristic molecular footprint, which is critical for the estimation of the total number of molecules being probed during SERS measurement and therefore a precise estimation of enhancement factor is possible. In order to determine the SERS activity of the Ag NPs containing alumina sols, 10 μL of MB solution of varying concentrations (1×10^{-4} to 1×10^{-12} M) and 10 μL of respective sol were homogeneously mixed to obtain a clear and transparent solution and from that 4 μL was drop cast. The Raman data

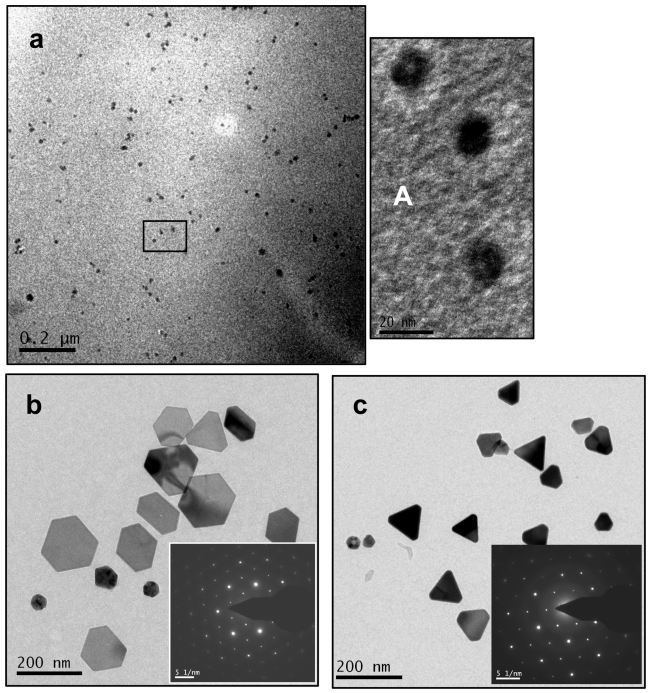

Figure 1. TEM images of the (a) yellow sol showing the presence of spherical Ag NPs having average size of about 12 nm; (A) magnified image of the rectangular area; (b) green sol showing mainly hexagonal Ag nanoplates (inset shows SAED taken from a hexagonal NP); (c) blue sol showing mainly truncated triangular nanoplates (SAED is given in the inset). SAED patterns shown in b and c confirm the single-crystalline nature of the nanoplates.

(using a Renishaw Invia Reflex system) were collected after exciting the samples with a 785 nm diode laser under line-focus mode and the laser power was adjusted to 0.5% which was about 1.25 mW. The laser was focused onto the sample surface using a 50× long working distance objective with a spot diameter of 1 μm (see the Supporting Information). Here long wavelength excitation (785 nm) was used which can avoid fluorescence background of organic dye molecules[21] and also to avoid photochemical degradation or transformation of adsorbed species. Spectra were collected at room temperature (~20 °C) in continuous mode with 10 s exposure time and accumulated for 1 time using a grating of 1200 mm^{-1}. In all cases, SERS spectra were acquired from 8−10 different places of the same samples and the median spectrum was reported. All SERS experiments were performed in triplicate to check the reproducibility of the whole process.

As the main absorption peaks of the MB located at around 656, 610, and 293 nm are away from the excitation wavelength (785 nm), the resonant Raman effect would be very weak.[21,22] From Figure 2a, it is clear that the characteristics Raman bands of MB alone (10^{-4} M) and MB with pure alumina sol (without Ag NPs) are too weak to be observed. The Raman spectra of MB adsorbed on Ag NPs in yellow, green and blue alumina sols are also presented in Figure 2a. As pointed out before, to check the uniformity of SERS, spectra were acquired from 10 different positions of same samples and a little variation in intensities was observed. As a representative example the intensity variation of the 445 cm^{-1} peak of MB for yellow, green and blue sols has been plotted and presented in Figure 2b. From this plot the respective median intensities have been chosen to report the corresponding spectra. As shown in Figure 2a, the

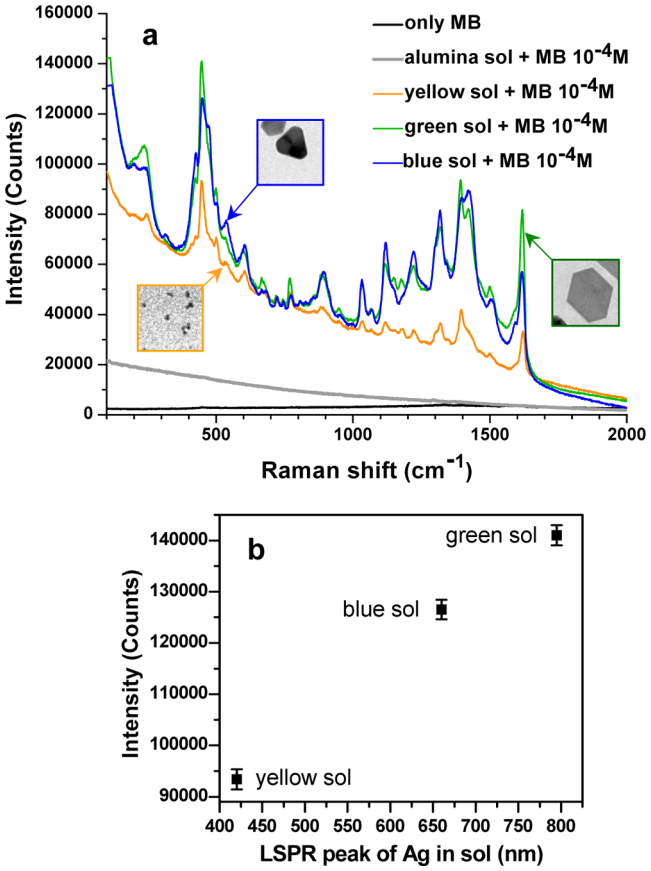

Figure 2. (a) Raman spectra of 1×10^{-4} M MB, 1×10^{-4} M MB adsorbed pure alumina sol (without Ag NPs), and SERS spectra of 1×10^{-4} M MB adsorbed on yellow, green, and blue sols; (b) intensity variation in 10 different measurements considering the 445 cm^{-1} peak (C−N−C skeletal bending) of MB for yellow, green, and blue sols.

characteristic Raman peaks at 1618 and 445 cm^{-1} due to the C−C stretching and C−N−C skeletal bending of MB,[23] respectively can be seen. This indicates that the MB molecules were well adsorbed on the substrates. The spectra of MB with yellow, green and blue colored sols exhibited remarkably stronger intensity due to the SERS effect. It can be observed that the spectral intensities obtained from the hexagonal and triangular nanoplates are much greater than the spherical NPs (Figure 2a, b). This reveals that the nanoplates are showing better SERS enhancement under the present experimental conditions. It may be noted here that no characteristic features of PVP was observed in the SERS spectra. Presence of PVP on the Ag NPs surface may have some effect on the binding of MB with Ag NPs.[24] As PVP binds preferentially on the {100} face of Ag, it is expected that {100} faces will be more occupied by PVP. Again, binding of positively charged MB with adsorbed PVP is unlikely.[25] So MB molecules will easily bind with the much exposed and abundant {111} faces of Ag nanoplates.

Figure 3 shows SERS of the Ag/alumina sols at different reaction stages during the gradual shape evolution of the Ag NPs. It shows nicely that at different longitudinal SPR (LSPR) peak positions (as shown in the UV−visible spectra, see Figure S1 in the Supporting Information; the sample collection sequence at different LSPR is also indicated in the body of the Figure 3) the intensity of SERS spectra gradually increases and reaches maximum value when sharp edged hexagonal NPs were formed. It is thus indicated that the generation of platelike thin

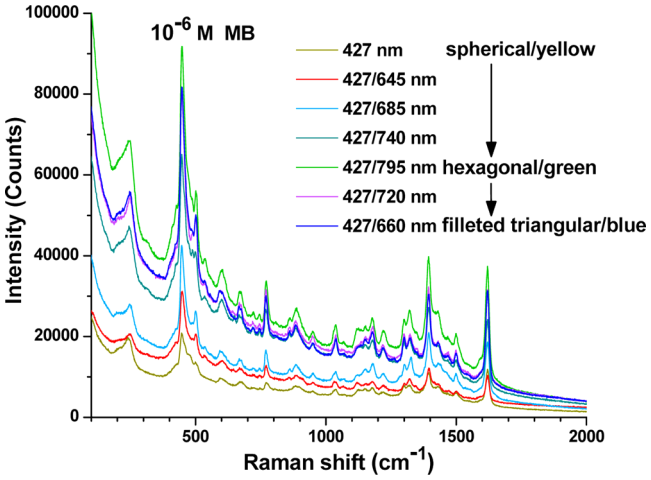

Figure 3. SERS evolution of 1×10^{-6} M MB adsorbed on the Ag doped alumina sol during the gradual shape conversion of the Ag NPs from spherical to hexagonal and finally filleted triangular nanoplates. The atomic concentration of Ag in the sol remains same throughout the shape evolution.

2D structure influences the Raman enhancement. After attaining the maximum enhancement the intensity again decreased slightly due to the formation of relatively thicker filleted triangular nanoplates (see Figures S3 and S4 in the Supporting Information).[17] Raman spectra of MB at very low concentrations adsorbed on green and blue alumina sols are shown in Figure 4. It is clear that the detection limit for MB on the hexagonal and filleted triangular nanoplates containing alumina could be 10^{-12} M or below, thus it can be used as a "fingerprint" to detect MB.

To estimate the SERS enhancement, we calculated the Raman enhancement factor (EF) per molecule as the ratio of the intensity in presence and absence of the active substrate.[26,27]

$$\mathrm{EF} = \frac{N_{\mathrm{bulk}}}{N_{\mathrm{ads}}} \frac{I_{\mathrm{SERS}}}{I_{\mathrm{Raman}}}$$

N_{bulk} is the number of analyte (MB) molecules in the focal volume. For N_{bulk} calculation, Raman spectrum of solid MB was used. N_{ads} is the number of molecules adsorbed on the SERS active substrate. This was calculated using the number of nanoparticles, the surface area of NPs, the number of analyte molecules estimated to be present and the monolayer surface coverage for MB.[26,27] I_{SERS} is the intensity of a vibrational mode in the surface enhanced spectrum and I_{Raman} is the intensity of same mode in the Raman spectrum. In our calculations the intensity of $\nu_{(\mathrm{C-N-C})}$ bending mode at 445 cm^{-1} was used to identify the enhancement factors. The calculated Raman EFs are 2.6×10^6, 1.2×10^9, and 8×10^8 for yellow, green and blue sols, respectively. Detailed EF calculations are given in the Supporting Information.

It is noteworthy that in colloidal solution, the spherical NPs and the shaped nanoplates move randomly due to Brownian motion. So when drop of the sol dries to form gel, the motion of the NPs ceases and the NPs freeze inside the alumina gel in a random orientation. So the SERS spectra are the representative of all possible orientations of the Ag NPs present inside the alumina gel under the laser spot.[28] Recently, Liu et al reported Raman enhancement on the order of 1×10^8 using vertically cross-linking Ag nanoplate arrays prepared by electrochemical

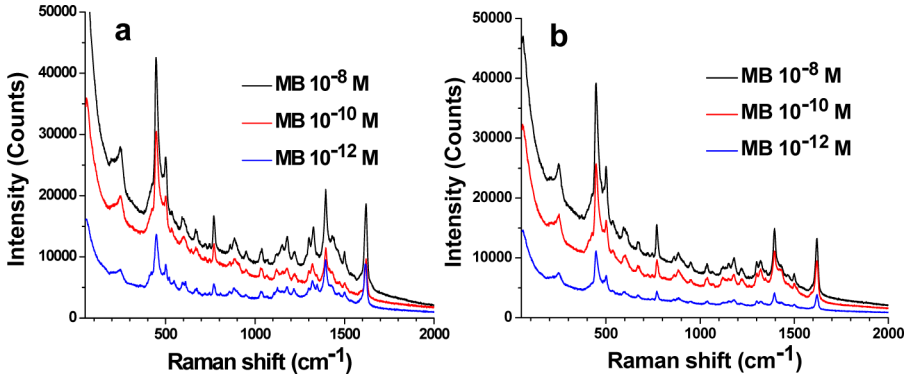

Figure 4. SERS spectra of different MB concentrations (1×10^{-8}, 1×10^{-10}, 1×10^{-12} M) adsorbed on (a) green and (b) blue alumina sols.

route.[29,30] Although these substrates are reusable, the overall process involves complicated techniques and seems to be disadvantageous from the practical application point of view. Using our randomly oriented Ag nanoplate embedded alumina sol, we obtained high Raman enhancement ($>1 \times 10^9$) with reproducibility.

Generally, it is believed that many factors simultaneously contribute to the Raman enhancement effect. The largest factor of SERS enhancement depends on the electromagnetic (EM) effect associated with large local fields due to resonances occurring in the microstructures on the metal surface.[31,32] It is known that variations in nanocrystal shape and dielectric environment can affect the surface polarization and alter the SPR. Here, both corner sharpness and shape symmetry alter the surface polarization and thus the SPR absorptions. Theoretical studies have suggested that the local field-effects in the NPs having sharp corners or edges can be enhanced by several orders of magnitude and responsible for SERS.[33,34] Here mainly, the sharp corners on the nanoplates in the green sol likely provide greater localized electric field enhancement than the rounded ones of the blue sol, thus resulting greater Raman enhancement.[35,36] Slight difference in enhancements of green and blue sol could be affected because of the amount of overlap of the SPR band and the excitation source. For the hexagonal nanoplates, the 785 nm laser falls near the SPR band (795 nm), whereas in the case of the truncated triangular nanoplates, the laser line is on the tailing edge of their SPR band (660 nm).[33] For spherical Ag NPs, the laser line is away from the SPR band (427 nm), which may be one of the reasons for their low Raman enhancement.

The embedding dielectric medium alumina can also play a vital role. It is known that when metal NPs are embedded in a high dielectric medium, alteration of SPR with significant enhancement of intensity is possible, which can contribute towards high Raman enhancement.[15,16,37,38] The nanoscale surface roughness of the nanoplates as observed by AFM (see Figure S3 in the Supporting Information) also contributes to a small proportion of the SERS enhancement.[15] As the Ag NPs are embedded in the alumina gel-like porous matrix, it can be expected that the NPs remain uniformly dispersed without any agglomeration or overlapping causing highest surface area available. Moreover, porous gel-like alumina matrix can easily hold the dye molecules. As a result, almost all the Ag NPs have a dye-rich environment, which in turn enhances the highest possible SERS effect.[39]

In summary, we have demonstrated a new and facile approach to produce very high Raman enhancement (order of magnitude $>1 \times 10^9$) using different shaped Ag NPs in alumina. Systematic SERS experiments were carried out in order to study the effect of nanoparticle−shape evolution in alumina with the SERS enhancement. It has been established that the LSPR due to the plate-shaped Ag NPs can be utilized to a large extent for SERS enhancement because of their dispersion and embedment in high dielectric alumina gel network where analyte molecules are held. This new approach gives uniform and strong SERS signal with reproducibility. Therefore, this reliable SERS technique can be utilized for various analytical applications.

■ ASSOCIATED CONTENT

Supporting Information

UV−visible spectral evolution and optical images of sols (Figure S1), particle size distributions of Ag NPs (Figure S2), AFM images and height scans of nanoplates (Figure S3), additional TEM images (Figure S4). and enhancement factor calculations. This material is available free of charge via the Internet at http://pubs.acs.org.

■ AUTHOR INFORMATION

Corresponding Author

*Tel: +91 33 23223403. Fax: +91 33 24730957. E-mail: gde@cgcri.res.in.

Notes

The authors declare no competing financial interest.

■ ACKNOWLEDGMENTS

DST, Government of India (Project SR/S5/NM-17/2006), and CSIR, India (Project NWP051) are thankfully acknowledged for providing funds. D.J. thanks CSIR for providing fellowship.

■ REFERENCES

(1) Zhang, B.; Wang, H.; Lu, L.; Ai, K.; Zhang, G.; Cheng, X. *Adv. Funct. Mater.* **2008**, *18*, 2348−2355.

(2) Wang, H. H.; Liu, C.Y.; Wu, S. B.; Liu, N. W.; Peng, C. Y.; Chan, T. H.; Hsu, C. F.; Wang, J. K.; Wang, Y. L. *Adv. Mater.* **2006**, *18*, 491−495.

(3) Laurier, K. G. M.; Poets, M.; Vermoortele, F.; Cremer, G. D.; Martens, J. A.; Uji-i, H.; Vos, D. E.; Hofkens, D. J.; Roeffaers, M. B. J. *Chem. Commun.* **2012**, *48*, 1559−1561.

(4) Xiao, X.; Nogan, J.; Beechem, T.; Montano, G. A.; Washburn, C. M.; Wang, J.; Brozik, S. M.; Wheeler, D. R.; Burckel, D. B.; Polsky, R. *Chem. Commun.* **2011**, *47*, 9858−9860.

(5) Zhang, M.; Zhao, A.; Sun, H.; Guo, H.; Wang, D.; Li, D.; Gan, Z.; Tao, W. *J. Mater. Chem.* **2011**, *21*, 18817−18824.

(6) Lin, Y.; Bunker, C. E.; Fernando, K. A. S.; Connell, J. W. *ACS Appl. Mater. Interfaces* **2012**, *4*, 1110−1117.
(7) Nie, S. M.; Emory, S. R. *Science* **1997**, *275*, 1102−1106.
(8) Fleischman, M.; Hendra, P. J.; Mcquillan, A. J. J. *J. Chem. Soc., Chem. Commun.* **1973**, 80−81.
(9) Zeisel, D.; Deckert, V.; Zenobi, R.; Vo-Dinh, T. *Chem. Phys. Lett.* **1998**, *283*, 381−385.
(10) Dick, L. A.; McFarland, A. D.; Haynes, C. L.; Van Duyne, R. P. *J. Phys. Chem. B* **2002**, *106*, 853−860.
(11) Lai, Y. C.; Pan, W. X.; Jhang, D. J.; Zhan, J. H. *Nanoscale* **2011**, *3*, 2134−2137.
(12) Ko, H.; Singamaneni, S.; Tsukruk, V. V. *Small* **2008**, *4*, 1576−1599.
(13) Chang, S.; Ko, H.; Singamaneni, S.; Gunawidjaja, R.; Tsukruk, V. V. *Anal. Chem.* **2009**, *81*, 5740−5748.
(14) Ko, H.; Chang, S.; Tsukruk, V. V. *ACS Nano* **2009**, *3*, 181−188.
(15) Ru, E. C. L.; Etchegoin, P. G. *Principles of Surface-Enhanced Raman Spectroscopy*, 1st ed.; Elsevier: Amsterdam, 2009, pp 362−364.
(16) Xu, J.; Kvasnička, P.; Idso, M.; Jordan, R. W.; Gong, H.; Homola, J.; Yu, Q. *Opt. Express* **2011**, *19*, 20493−20505.
(17) Jana, D.; De, G. *J. Mater. Chem.* **2011**, *21*, 6072−6078.
(18) The detailed UV−visible spectral evolution, TEM studies, and shape conversion mechanism have been reported in ref 17. In that work, diluted sol droplets were used to observe the TEM, and we found one or two particles in one frame. In this work, TEM studies were done in a different way to show maximum number of particles. For this purpose, green and blue alumina sols were centrifuged at 10 000 rpm for 10 min and the centrifuged product was washed with 1-propanol and one small drop of the diluted solution of the precipitate was used for TEM study after drying.
(19) Sun, Y.; Mayers, B.; Herricks, T.; Xia, Y. *Nano Lett.* **2003**, *3*, 955−960.
(20) Atherton, S. J.; Harriman, A. *J. Am. Chem. Soc.* **1993**, *115*, 1816−1822.
(21) Xiao, G.-N.; Man, S.-Q. *Chem. Phys. Lett.* **2007**, *447*, 305−309.
(22) Camargo, P. H. C.; Au, L.; Rycenga, M.; Li, W.; Xia, Y. *Chem. Phys. Lett.* **2010**, *484*, 304−308.
(23) Naujok, R. R.; Duevel, R. V.; Corn, R. M. *Langmuir* **1993**, *9*, 1771−1774.
(24) Pinkhasova, P.; Yang, L.; Zhang, Y.; Sukhishvili, S.; Du, H. *Langmuir.* **2012**, *28*, 2529−2535.
(25) Pinto, J. R.; Novak, S. W.; Nicholas, M. *J. Phys. Chem. B* **1999**, *103*, 8026−8032.
(26) Félidj, N.; Aubard, J.; Lévi, G.; Krenn, J. R.; Salernon, M.; Schider, G.; Lamprecht, B.; Leitner, A.; Aussenegg, F. R. *Phys. Rev. B* **2002**, *65*, 075419.
(27) Hunyadi, S. E.; Murphy, C. J. *J. Mater. Chem.* **2006**, *16*, 3929−3935.
(28) Tiwari, V. S.; Oleg., T.; Darbha, G. K.; Hardy, W.; Singh, J. P.; Ray, P. C. *Chem. Phys. Lett.* **2007**, *446*, 77−82.
(29) Liu, G.; Cai, W.; Kong, L.; Duan, G.; Lü, F. *J. Mater. Chem.* **2010**, *20*, 767−772.
(30) Liu, G.; Cai, W.; Kong, L.; Duan, G.; Li, Y.; Wang, J.; Zuo, G.; Cheng, Z. *J. Mater. Chem.* **2012**, *22*, 3177−3184.
(31) McFarland, A. D.; Young, M. A.; Dieringer, J. A.; Vanduyne, R. P. *J. Phys. Chem. B* **2005**, *109*, 11279−11285.
(32) Moskovits, M. *Rev. Mod. Phys.* **1985**, *57*, 783−826.
(33) Mclellan, J. M.; Siekkinen, A.; Chen., J.; Xia, Y. *Chem. Phys. Lett.* **2006**, *427*, 122−126.
(34) Zou, S.; Schatz, G. C. *Chem. Phys. Lett.* **2005**, *403*, 62−67.
(35) Rycenga, M.; Kim, M. H.; Camargo, P. H. C.; Cobley, C.; Li, Z.-Y.; Xia, Y. *J. Phys. Chem. A* **2009**, *113*, 3932−3939.
(36) Kelly, K.; Coronado, E.; Zhao, L.; Schatz, G. C. *J. Phys. Chem. B* **2003**, *107*, 668−677.
(37) Lizárraga, R.; Holmström, E.; Parker, S. C.; Arrouvel, C. *Phys. Rev. B* **2011**, *83*, 094201.
(38) Kingon, A. I.; Maria, J.-P.; Streiffer, S. K. *Nature* **2000**, *406*, 1032−1037.
(39) Chan, S.; Kwon, S.; Koo, T. W.; Lee, L. P.; Berlin, A. A. *Adv. Mater.* **2003**, *15*, 1595−1598.